LNF-91/090

APPLICATION of IMPROVED AREA DETECTOR FOR CONTINUOUS SMALL ANGLE X-RAY SCATTERING USING SYNCHROTRON RADIATION

A. La Monaca, M. Barteri, E. Borghi, A. Congiu - Castellano, G. Cappuccio, M. Beltramini, A. Salvato, J. S. Shah

estratto da
Nucl. Instr. & Meth. A310(1991) 403-410

Nuclear Instruments and Methods in Physics Research A310 (1991) 403–410
North-Holland

NUCLEAR
INSTRUMENTS
& METHODS
IN PHYSICS
RESEARCH
Section A

Application of the improved area detector for continuous small angle X-ray scattering using synchrotron radiation

Andrea La Monaca
INFN, Laboratori Nazionali di Frascati, P.O. Box 13, 00044 Frascati, Italy

Mario Barteri and Elena Borghi
Dip. di Chimica, Università "La Sapienza", Roma, Italy

Agostina Congiu-Castellano
Dip. di Fisica, Università "La Sapienza", Roma, Italy

Giorgio Cappuccio
CNR-INFN, Istituto di Strutturistica Chimica Monterotondo Sc., Roma, Italy

Mariano Beltramini and Benedetto Salvato
Dip. di Biologia, Università di Padova, Padova, Italy

Jitendra Shantilal Shah
H.H. Wills Physics Laboratory, University of Bristol, Bristol BS8 1TL, UK

Continuous small angle X-ray scattering experiments were performed on high molecular weight proteins, hemocyanins and transferrins, with the Frascati drift chamber area detector and the diffraction camera. The detector used the time structure of Adone synchrotron radiation for operating a faster data acquisition system with real time graphics for monitoring and interpreting scattering data. The diffraction camera with the relative angular resolution $\Delta k/k$ of 0.12 could measure a minimum scattering momentum k_{min} of 8×10^{-3} Å^{-1}. Preliminary results obtained on lyophilized half-met hemocyanin and transferrins indicate formation of clusters. Small angle X-ray scattering data on the native hemocyanin is in agreement with the model (a hollow cylinder) derived from electron microscopy.

1. Introduction

We have developed a small angle X-ray diffraction apparatus incorporating a gas drift chamber X-ray position sensitive detector to be used with the Frascati Synchrotron Wiggler source with a fast computerized data acquisition system. The parameters pertaining to the detector and the resolution of the diffraction apparatus were reported recently [1,2]. We have used the above system for studying proteins: lyophilized hemocyanin from the mollusc Octopus V. and human transferrins.

Hemocyanins are specific oxygen-carrier proteins found as extracellular oligomers of high molecular weight in the hemolymph of several species of *Mollusca* and *Arthropoda*. There are basically three morphological classes of hemocyanins, called 102S, 57S and 49S. They are classified and distinguished according to their sedimentation coefficients and dissociation–association behaviour. The 102S represents the basic structure of the class Gastropoda. The 57S and 49S represent the whole molecule of hemocyanins of Decapoda and Octopoda classes respectively. Although 57S and 49S varieties are being studied by a number of different techniques their structure is not known in any great detail. A model for the structure of the 102S hemocyanin has been proposed from observation by electron microscopy [3,4].

Human serum transferrin is a glycoprotein, responsible for iron transport to red blood cells which synthesize hemoglobin. The iron uptake by the metal depleted form (known as apo-transferrin) occurs in two

different site of binding giving the mono and diferric transferrins. Binding of Fe causes conformation changes in the molecule. Apo, mono and diferric transferrins have been studied by small angle X-ray scattering and the measurements indicate that they have a prolate (elongated) spheroidal molecular shape [5]. Small angle neutron scattering data on the other hand suggest that the molecules have oblate (flattened) spheroidal shapes [6].

2. Apparatus

The drift chamber area detector is shown in fig. 1. (The full specifications of the detector are given in table 1). It is comparatively immune from radiation damage and has uniform sensitivity of detection, wide dynamic range and high spatial resolution. Fig. 2 shows the detected intensity profile of a beam through a pinhole of diameter 110 μm placed at 500 mm from the detector.

This confirms that the spatial resolution of the detector in both dimensions is at least 155 μm. This high resolution in both dimensions (i.e. drift coordinate and delay line coordinate) is due to the following reasons: (1) the drift chamber uses the time structure of Adone synchrotron radiation for measuring drift coordinate; (2) delay time, delay rise time, band pass width and attenuation coefficient have been improved. The maximum count rate of the detector is also better than before (0.7 MHz) because the detector uses a semicylindrical cathode and a small gap between the cathode and the anode. To take advantage of this the detector was connected to a fast data acquisition system. Fig. 3 schematically shows the whole experimental arrangement including the data acquisition system. As can be seen the system is controlled through a Macintosh IIx computer which, through a VME bus, controls the CAMAC, time to digital converters connected to the detector, and the associated histogram memories. The data is displayed in real time by a software written in the real time Fortran language developed at CERN.

For obtaining small angle scattering patterns the detector was mounted at the back of a pinhole collimator system and the camera, at 35 m from the actual wiggler source. The diffraction camera with its collimation system is shown in fig. 4 and its characteristic parameters are given in table 2 (further details of the systems have been reported elsewhere [1,2,7]).

With this apparatus it is possible to use different pinhole diameters, for collimation, in the range 0.11–1.2 mm, to produce a circular primary beam. For reducing parasitic scattering a second pinhole is used. For hemocyanin and transferrin protein measurements we used a pinhole combination of diameters 0.5 mm and 0.7 mm. The relative angular resolution of the camera was $\Delta k/k = 0.12$. The minimum scattering momentum k_{min} that could be measured with our system was 8×10^{-3} Å^{-1}. During the actual measurements biological solutions and lyophilized samples were kept

Fig. 1. Photograph of the drift chamber detector.

in miniaturized cells to stop evaporation and change of density.

3. Materials and preparation

Human serum apo-transferrin was purchased from Sigma Chemical Company and used without further purification. We have prepared diferric transferrins by reacting apo-protein with $FeCl_3$ at pH 7.4 (tris buffer) in presence of equimolar bicarbonate ions. The samples have been used lyophilized.

Octopus V. native hemocyanin has been purified and converted to the half-met form by nitrite treatment from the deoxyprotein. Samples of oxy-hemocyanin and half-met hemocyanin have been used as dry powders after lyophilization with sucrose 1:2 w/w.

4. Experimental results

Fig. 5 shows small angle X-ray scattering patterns of the specimens. The patterns were taken over a period of 10 to 30 min. In our system the detector plane is placed to record only one half of the symmetric scattering pattern on one side of the equatorial plane. To calibrate the performance of the detector and the diffraction apparatus *a standard 'lupolen' specimen*

Table 1
Drift chamber area detector specifications

Performances:	
Quantum efficiency with $\lambda = 1.54$ Å and using Ar or Xe mixtures	20–84 %
Active area	17×20 mm^2
Spatial resolution: X(drift)$\times$ Y(delay)	120×155 μm^2
Pixel number	142×129 pixels
Maximum storage of the buffer memories	256×256 pixels
Maximum counting rate for each pixel	2.2×10^4 cps
Maximum count capability of detector	1×10^6 cps
Maximum linear count of the whole system	7×10^5 cps
Construction:	
Overall dimensions: cylindrical body (diameter/height)	200 75 mm
Detector volume	$30 \times 20 \times 10$ mm^3
Grid: Be–Cu silvercote tempered wires, diameter	101 μm
Anode: W gold plated wire with 3% Re, diameter	20 μm
Anode gap	2.4 mm
Semicylindrical cathode: Cu, diameter	6 mm
Window material: mylar sheet	24 μm
Delay-line parameters:	
Active length $\times$ width	2.93×3.57 mm
Dielectric insulation thickness	12 μm
Wire section	50 μm
Windings	172 turns/cm
Impedance	1950 Ω
Coupling efficiency	22 %
Delay	116 ns/cm
Delay/risetime	10.5
Attenuation	0.35 dB/cm
Band pass	2.75 MHz/cm
Bias voltage:	
Drift field	−3000 V
Grid & semicylindrical cathode	+50 V
Anode	+1600 V
Cathode plate	ground potential
Gas mixtures ($T = 20$ °, $P = 1000$ mbar):	
Ar/Isob/Methylal (or Xe/CO_2)	66/30/4 (or 80/20)%
Front-end electronics:	
Emitter followers and low level amplifier comparators connected to the sense wire and to the delay line ends.	

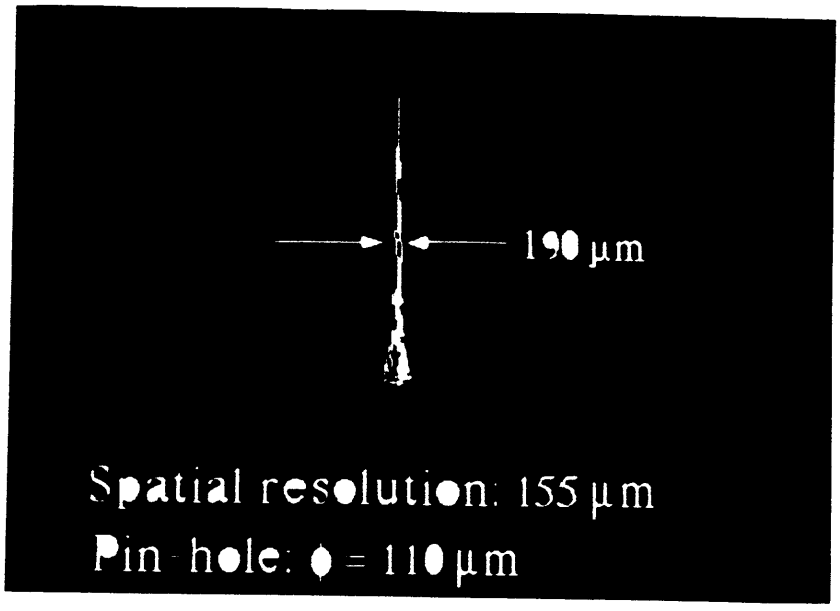

Fig. 2. Intensity profile of the beam passed through a pinhole of diameter 110 μm.

(amorphous platelet of polyethylene with 35% crystallinity) was placed in the beam so that its preferential crystalline direction was as near the equatorial direction as possible. Fig. 5a shows lupolen scattering pattern. The anisotropy of the scattered intensity due to the presence of preferential direction of crystallinity is evident therein. The anisotropy in the pattern was obvious right from the beginning of collection of the data and could be seen in real time. The radius of gyration deduced from the analysis of the intensity curves was 116 Å. The dimension of the scattering units was found to be 150 ± 2 Å. This agrees well with the published data.

Figs. 5b, 5c and 5d show the patterns of lyophilized apo-transferrin, native and half-met hemocyanin. It is interesting to note that they too show an asymmetric distribution of intensity but the higher intensity is on the right-hand side of the meridian, while the lupolen

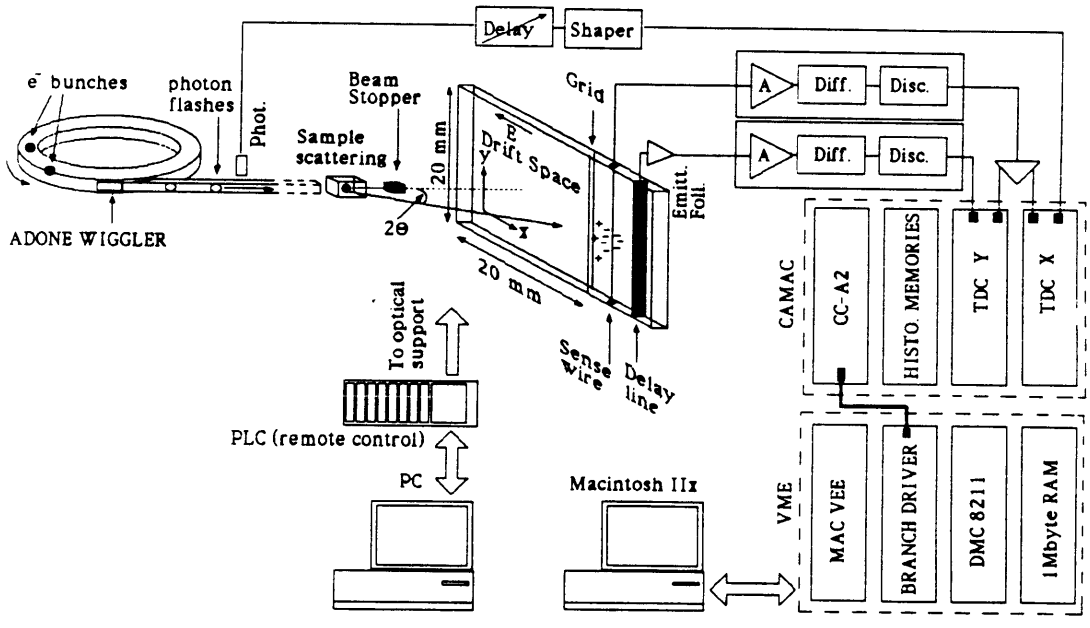

Fig. 3. Diagram of the overall configuration of the diffraction experiment with respect to the ADONE wiggler source.

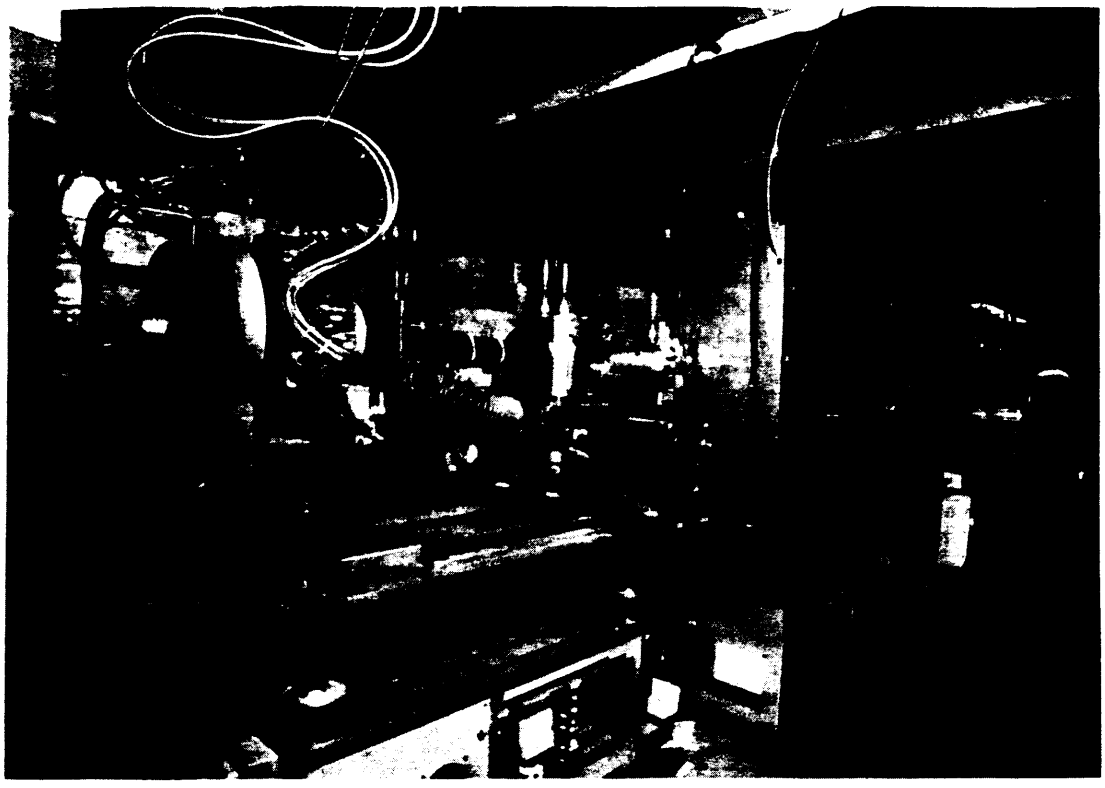

Fig. 4. Photograph of the Small Angle X-ray Scattering (SAXS) apparatus.

pattern has it on the left-hand side. This indicates that there may be a direction of preference with respect to the concentration of the scattering units in our preparations. This clearly requires further investigation. Figs. 6 and 7 show Guinier plots of the mean scattering curves obtained from the patterns in figs. 5b, 5c and

Table 2
Characteristics of SAXS apparatus

Source: wiggler insertion device, Adone in single bunch	
Electron bunch current	30 mA
Bunch time interval, T	351 ns
Bunch time duration, Δt	< 1 ns
X-ray light beam wavelength, λ (with $\Delta\lambda/\lambda = 10^{-4}$)	1.54 Å
Diameter of pinhole collimator (variable [a])	0.5 mm
Primary beam angular divergence: $2\alpha_h \times 2\alpha_v$ [b]	76″-6″
Cross section of the beam at specimen: $h_h \times h_v$ [b]	0.68×0.51 mm^2
Intensity on the sample, I	2.4×10^7 ph/sec
Conical angle of parasitic scattering $2\theta'$	412″
Max. and min. specimen–detector distance d:	500–40 mm
Max. angle obscured by the beam-stopper 2θ	227″
Angular range covered by the detector at max. and min. distance	2°-25°
Angular range covered by the goniometer at max. and min. distance	25°-134°
Max. and min. angular resolution on the detector plane: $\Delta(2\theta)_h$ [b]	50″-618″
Max. and min. angular resolution on the detector plane: $\Delta(2\theta)_v$ [b]	66″-825″
Min. scattering momentum: k_{min}	8×10^{-3} Å^{-1}
Max. observable dimension of the scattering unit D	785 Å
Relative angular resolution: $\Delta k/k$	0.12

[a] A sets variable pinholes in the range 0.11–1.2 mm is valuable to improve some particular experimental parameter.
[b] h = horizontal, v = vertical.

5d. Table 3 lists all the parameters of the specimens calculated from the Guinier plots. It is evident that in half-met hemocyanin there are distinctly two scattering units of different dimensions.

5. Discussion

The model of native 49S hemocyanin [4], derived from electron microscopy, is a hollow cylinder with an internal diameter of 200 Å and an external diameter of 300 Å. The height is about 170 Å [3]. The dimensions given by small angle scattering of Octopus hemocyanin specimens (table 3) appear to be reasonable.

In case of half-met hemocyanin the measurements clearly show two sets of radii of gyration. The smaller radius corresponds to a primary scattering unit and the greater set corresponds to some kind of cluster formation. The primary scattering unit as derived from the data has dimensions which are very different to that of the native hemocyanin.

6. Conclusions

This study has conclusively shown that the small angle scattering apparatus with the improved drift chamber area detector is extremely useful for deriving accurate structural data. In our view fast response time of the detector and the ability of viewing the data in real time opens up exciting possibilities of studying changes in the structure and form due to a variety of causes such as chemical reaction, mechanical stress.

Acknowledgements

We wish to thank Dr. A. Stecchi of INFN-LNF for help given on preparing software for graphic elaboration of data, Dr. H.J. Sanchez of Facultad de Matematica, Astronomia y Fisica, Universitad Nacional de Cordoba (Argentina), for helpful discussion and his collaboration during the execution of experiment, PWA group of INFN for the provision of the Adone wiggler beam line, and the "Gruppo V" of INFN for financial support (FADD project).

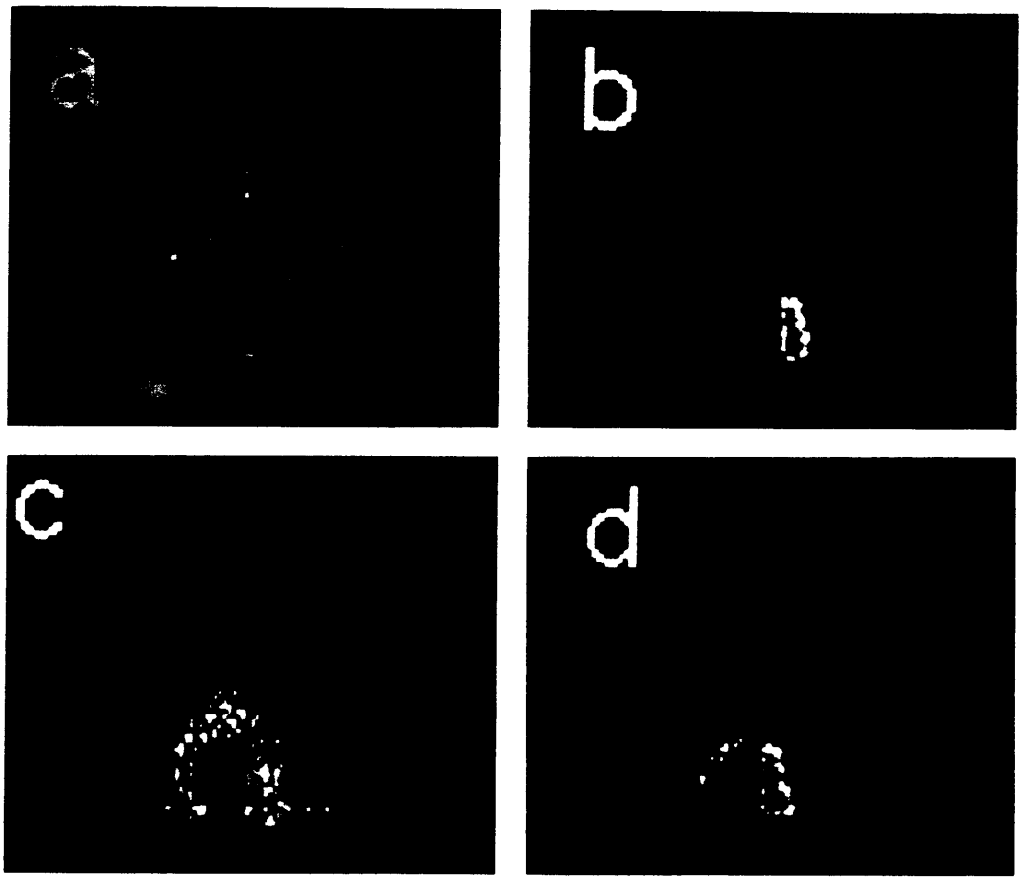

Fig. 5. (a) lupolen; (b) apo-transferrin; (c) native hemocyanin; (d) half-met hemocyanin.

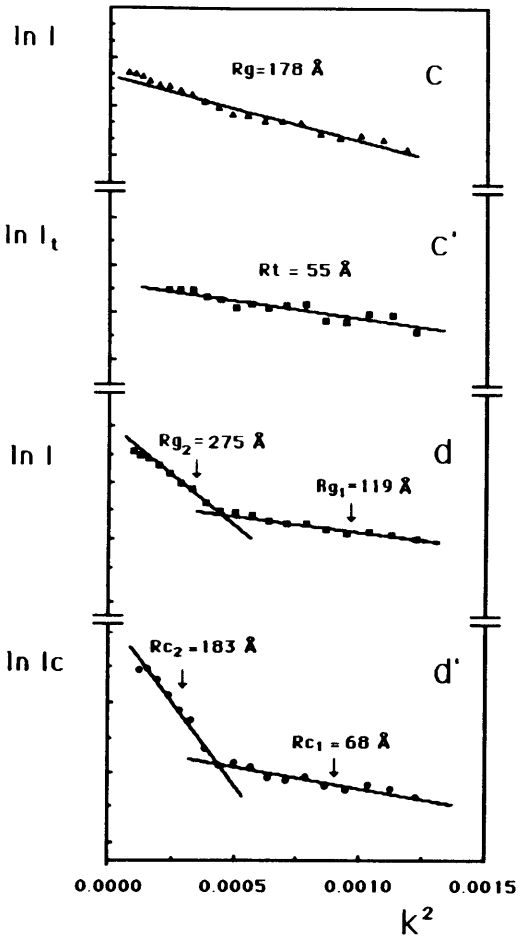

Fig. 6. Guinier plot of mean scattering curves obtained from experimental diffraction patterns: (c) average radius of gyration (Rg) and (c') radius of gyration corresponding to the thickness (Rt) of the scattering units of native hemocyanin; (d) average radii of gyration (Rg1 and Rg2) and (d') radii of gyration of the cross section (Rc1 and Rc2) of half-met hemocyanin.

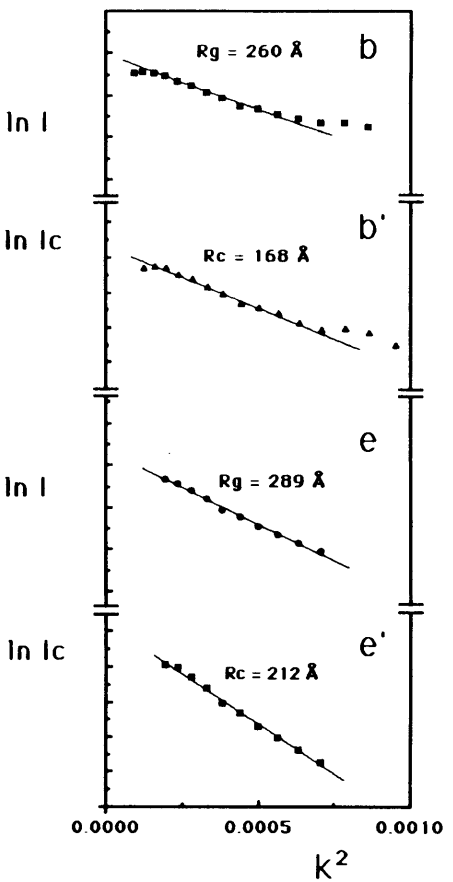

Fig. 7. Guinier plot of mean scattering curves obtained from experimental diffraction patterns: (b) average radius of gyration (Rg) and (b') radius of gyration of the cross section (Rc) of apo-transferrin; (e) average radius of gyration and (e') radius of gyration of the cross section (Rc) of diferric transferrin.

Table 3
Anisometric parameters of the Octopus hemocyanin and human transferrin proteins obtained by the Adone SAXS camera [a]

Native Hc sample c	Half-met Hc sample d	Apo-Trf sample b	Trf-$[Fe]_2$ sample e
Molecule:	i) Molecule:	Cluster:	Cluster:
R_g = 178 Å	R_{g1} = 119 Å	R_g = 260 Å	R_g = 288 Å
R_c = 169 Å	R_{c1} = 68 Å	R_c = 168 Å	R_c = 212 Å
R_t = 55 Å			
$V_i = (252 Å)^3$	$V_i = (128 Å)^3$	$V_i = (538 Å)^3$	$V_i = (680 Å)^3$
Model:	Model:	Model:	Model:
hollow cylinder	elliptic cylinder	rod-like shape	oblate shape
l = 191 Å	l = 338 Å	l = 687 Å	l = 675 Å
d_i = 246 Å	d_i = 60 Å	a = 551 Å	a = 897 Å
d_e = 408 Å	d_2 = 130 Å	b = 411 Å	b = 519 Å
t_w = 81 Å			
	ii) Cluster:		
	R_{g2} = 275 Å		
	R_{c2} = 183 Å		
	$V_{i2} = (519 Å)^3$		
	Model:		
	rod-like shape		
	l = 711 Å		
	a = 626 Å		
	b = 314 Å		

[a] Legenda: R_g = gyration radius; R_c = gyration radius of the cross section; R_t = gyration radius of the thickness; V_i = invariant volume; l = length; d_i, d_e = internal and external diameters; t_w = thickness of the wall; d, d_2 = diameters of the cross section of the elliptic cylinder; a, b = dimensions of the cross section of the cluster.